THE PENNSYLVANIA STATE UNIVERSITY
SCHREYER HONORS COLLEGE

DEPARTMENT OF MATHEMATICS

THE PROPAGATION OF SHALLOW-WATER WAVES

MARK EDWARD WALSH
Spring 2011

A thesis
submitted in partial fulfillment
of the requirements
for a baccalaureate degree
in Physics
with honors in Mathematics

Reviewed and approved* by the following:

Diane Henderson
Professor of Mathematics
Thesis Supervisor/Honors Adviser

Nigel Higson
Evan Pugh Professor of Mathematics
Faculty Reader

* Signatures are on file in the Schreyer Honors College.

Abstract

In this thesis, we look at the propagation of shallow-water waves using theory, experiment, and ocean data. First, we examine the classical models for shallow-water waves and look for approximate solutions to the initial value problem. Second, we use the theory as a framework for experiments and for data collected from tsunamis. Third, we qualitatively compare the results obtained from laboratory experiments and ocean data to predictions. We find that these predictions are in qualitative agreement with both the experimental data and the ocean data. However, predictions of actual tsunami evolution at particular locations require knowledge of the initial data, which is not known in real time, and knowledge of bathymetry, which we do not account for herein.

Table of Contents

1. Introduction

Before 1834, the prevailing theory governing water waves were Newton's and Bernoulli's theories of hydrodynamics. These theories asserted that all waves dispersed into a train of oscillatory motions. However, in 1834, John Scott Russell observed a wave that ran contrary to this theory:

"I believe I shall best introduce this phenomenon by describing the circumstances of my own first acquaintance with it. I was observing the motion of a boat which was rapidly drawn along a narrow channel by a pair of horses, when the boat suddenly stopped – not so the mass of water in the channel which it had put in motion; it accumulated round the prow of the vessel in a state of violate agitation, then suddenly leaving it behind, rolled forward with great velocity, assuming the form of a large solitary elevation, a rounded, smooth, and well-defined heap of water, which continued its course along the channel apparently without change of form or diminution of speed. I followed it on horseback, and overtook it still rolling on at a rate of some eight or nine miles per hour, preserving its original figure some thirty feet long and a foot to a foot and a half in height. Its height gradually diminished, and after a chase of one or two miles I lost it in the windings of the channel. Such, in the month of August 1834, was my first chance interview with that singular and beautiful phenomenon which I have called the *Wave of Translation*, a name which it now very generally bears; when I have since found to be an important element in almost every case of fluid resistance, and ascertained to be the type of that great moving elevation of the sea, which, with the regularity of a planet, ascends our rivers and rolls along our shore." – John Scott Russell (1834)

This observation had not been recorded before this; the prevailing theories could not explain a wave that did not disperse into a train of waves. Inspired by this observation, Russell was able to reconstruct this observation in his laboratory. However, it was not until the 1870s that theories were proven to support these experimental observations; these theories created a fresh look at the theory of water waves.

In this paper, we explore the theory of wave propagation in shallow water. These waves occur when the water depth is much less than the wavelength of the propagating wave. As we will see, the speed of these waves is based on the depth of the water, rather than on the frequency. By studying these waves through theory and experiment, we can better understand the propagation of long waves in the ocean, including tsunamis.

2. The Boundary-Value Problem for Water Waves

A boundary-value problem for water waves comes from the Stokes (1847) formulation for water waves. This model assumes incompressible, irrotational flow in an inviscid fluid (water) in contact with air. We neglect the interactions of water and air so that the interface is a free boundary. Figure 1 shows a schematic of the fluid domain, where h is the depth of the water and $\eta(x,t)$ is the location of the surface.

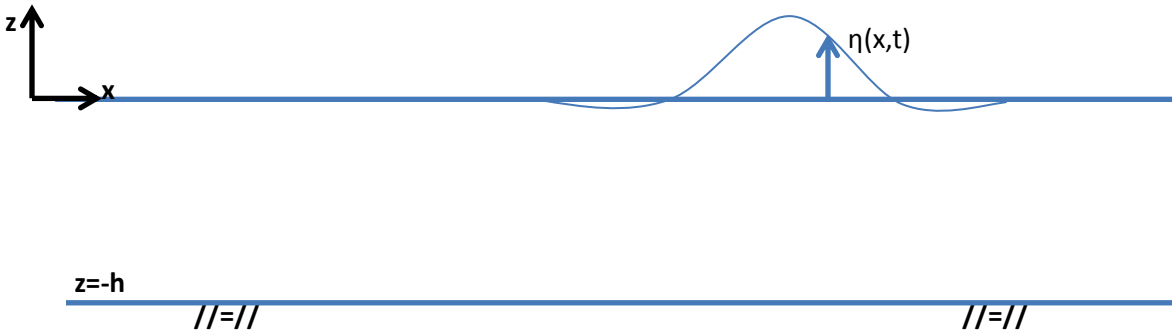

Figure 1: Schematic of fluid domain for Stokes formulation

Under the above assumptions we can express the flow velocity in terms of a velocity potential $\Phi(x,z,t)$. Then the governing equation throughout the fluid domain comes from the conservation of mass, which gives Laplace's equation,

$$\nabla^2\Phi = 0. \tag{2.1}$$

We allow the flow to be infinite in the horizontal extent. Then the boundary condition at the bottom is no flow through the bottom surface, such that

$$\Phi_z = 0 \qquad \text{on } z = -h, \tag{2.2}$$

where we neglect depth variations. There are two boundary conditions at the free surface: a kinematic and a dynamic boundary condition. The kinematic boundary condition defines the surface of the water, so that

$$\eta_t - \Phi_z + \eta_x\Phi_z = 0 \qquad \text{on } z = \eta(x,t). \tag{2.3}$$

The dynamic condition allows for a gravitational restoring force and states that there is no jump in pressure at the interface between the air and the water. Therefore, we require

$$\Phi_t + g\eta + \tfrac{1}{2}\nabla\Phi\cdot\nabla\Phi = 0 \qquad \text{on } z = \eta(x,t). \tag{2.4}$$

We begin by linearizing the problem to build intuition about the behavior of waves under the assumption of small surface displacements η, small wave slopes η_x, and correspondingly small wave velocities $\nabla\Phi$. The linearized problem is (2.1), (2.2), and

$$\eta_t - \Phi_z = 0 \qquad \text{on } z = 0 \qquad (2.5)$$

$$\Phi_t + g\eta = 0 \qquad \text{on } z = 0. \qquad (2.6)$$

Following Dean and Dalrymple (1991), we can solve the linearized problem by separation of variables. We look for a solution of the form

$$\Phi(x, z, t) = F(x)G(z)H(t). \qquad (2.7)$$

Then (2.1) becomes

$$F''(x)G(z)H(t) + F(x)G''(z)H(t) = 0. \qquad (2.8)$$

After algebraic manipulation, we obtain

$$F''(x)G(z) = -F(x)G''(z), \qquad (2.9)$$

and finally,

$$\frac{F''(x)}{F(x)} = -\frac{G''(z)}{G(z)} = \lambda, \qquad (2.10)$$

where λ is the separation constant. It is constant because the left side of the equation is a function of x, and the right side is a function of z. In order for these functions to be equivalent, they must both be equal to a constant. Also, we will choose the constant to be negative, to obtain wave propagation in the x-direction. We use $\lambda = -k^2 < 0$ and obtain an ordinary differential equation (ODE) for x-dependence,

$$F''(x) + k^2F(x) = 0. \qquad (2.11)$$

The solution to (2.11) is

$$F(x) = A\cos(kx) + B\sin(kx), \qquad (2.12)$$

where A and B are arbitrary constants.

We substitute $\lambda = -k^2$ into (2.10) and determine that $G(z)$ must satisfy

$$G''(z) - k^2G(z) = 0. \qquad (2.13)$$

The solution to (2.13) is

$$G(z) = C\cosh[k(z+h)] + D\sinh[k(z+h)], \qquad (2.14)$$

where C and D are also arbitrary constants.

To satisfy the bottom boundary condition (2.2), $G'(z) = 0$, on $z = -h$. Then

$$G'(z) = Ck\sinh[k(z+h)] + Dk\cosh[k(z+h)], \qquad (2.15)$$

and at z=-h,

$$G'(-h) = Ck\sinh(0) + Dk\cosh(0) = 0. \tag{2.16}$$

We know that $\sinh(0) = 0$ and $\cosh(0) = 1$, therefore, by the Zero Product Rule, $Dk = 0$, which implies that $D = 0$ (because $k^2 > 0 \Rightarrow k \neq 0$). So,

$$G(z) = C\cosh[k(z+h)]. \tag{2.17}$$

Based upon our solutions for $F(x)$ and $G(z)$, we obtain

$$\Phi(x,z,t) = [A\cos(kx) + B\sin(kx)]\,C\cosh(k[z+h])H(t). \tag{2.18}$$

In order to determine H(t), we use (2.6). Taking the time derivative of each side, we get

$$\Phi_{tt} = -g\eta_t \text{ on } z = 0. \tag{2.19}$$

We use (2.5) with (2.19) to obtain

$$\Phi_{tt} + g\Phi_z = 0. \tag{2.20}$$

Substituting (2.18) into (2.20), and using

$$\Phi_z = F(x)H(t)[Ck\sinh(kh)] \qquad \text{on } z = 0, \tag{2.21}$$

and

$$\Phi_{tt} = F(x)H''(t)[C\cosh(kh)] \qquad \text{on } z = 0, \tag{2.22}$$

we obtain a second order ODE for the time dependence, $H(t)$, of Φ, which is

$$H''(t) + gh\tanh(kh)H(t) = 0. \tag{2.23}$$

We define a radian frequency, ω, such that $\omega^2 := gk\tanh(hk)$, and (2.23) has the solution

$$H(t) = E\cos(\omega t) + F\sin(\omega t), \tag{2.24}$$

where E and F are arbitrary constants.

We find $\eta(x,t)$ using (2.5). Taking the z-derivative of Φ, we obtain

$$\Phi_z = F(x)H(t)[Ck\sinh(kh)]. \tag{2.25}$$

Using (2.5), we integrate with respect to t to find

$$\eta_t = F(x)[Ck\sinh(kh)]\,H(t), \tag{2.26}$$

$$\eta(x,t) = F(x)[Ck\sinh(kh)]\int H(t)dt, \tag{2.27}$$

$$\eta(x,t) = F(x)[Ck\sinh(kh)]\,[\frac{E}{\omega}\sin(\omega t) + \frac{F}{\omega}\cos(\omega t)]. \tag{2.28}$$

Using trigonometric identities and restricting the system to allow for right-running waves only, we obtain

$$\eta(x,t) = a_0\cos(kx - \omega t). \tag{2.29}$$

The arbitrary constant a_0 is the wave amplitude, and the velocity potential is

$$\phi(x,z,t) = \frac{a_0\omega}{k\sinh(hk)}[\sin(kx-\omega t)][\cosh[k(z+h)]]. \tag{2.30}$$

Here we are studying tsunamis, for which wave lengths are long compared to water depth, so that $kh = \frac{2\pi h}{L} \ll 1$, where L is a typical wavelength. This is the shallow-water limit for water waves. In this limit, $\tanh(kh) \to kh$, so $\omega^2 = gk^2h$. The phase speed of the wave is ${c_0}^2 := \frac{\omega^2}{k^2} = gh$. Therefore, $c_0 = \sqrt{gh}$ is the approximate speed of waves in shallow water. This approximation corresponds to zero dispersion; that is, the phase speed of the wave does not depend on the wavelength.

3. A Model Problem – The KdV Equation

In this section, we approximate the boundary problem (2.1)-(2.4) by taking into account the effects of weak nonlinearity and weak dispersion. We then examine how these factors affect the wave behavior and evolution, in the cases where they are invoked separately and when both are present. These solutions are examined both near the front of the traveling wave and in the region trailing the wave.

3.1 Solitons and the KdV Equation

The Stokes formulation of the surface boundary value problem (2.1)-(2.4) is a set of nonlinear partial differential equations (PDEs) with boundary conditions at the unknown free surface. In section 2, we linearized and neglected dispersion by invoking the limit $\tanh(kh) \to kh$.

Here, we allow for both weak nonlinearity and weak dispersion. We include weak dispersion by including the first two terms of the Taylor series for $\tanh(kh)$, so that $\tanh(kh) \to kh + \frac{1}{3!}(kh)^3$. By allowing weak nonlinearity also one can derive (see Ablowitz and Segur, 1981) the Korteweg-deVries (KdV) equation, which is an evolution equation for wave amplitudes. This equation provides us with a model for tsunami propagation.

A nondimensional version of the KdV equation is

$$u_\tau + 6uu_\chi + u_{\chi\chi\chi} = 0, \tag{3.1}$$

where $u(\chi, \tau) = \frac{3}{2h}\eta$ corresponds to the amplitude of the wave and where $\tau = \varepsilon \frac{c_0}{6h} t$ and $\chi = \varepsilon \frac{1}{h}(x - c_0 t)$ are slow variables in terms of a small parameter $\varepsilon \ll 1$. So, (3.1) describes the slowly varying evolution of wave amplitudes.

Here we look for solutions of (3.1), following Strauss (2008), corresponding to the dispersionless wave of elevation observed by J.S. Russell as described in Section 1. His wave was a traveling wave, so we require

$$u(\chi, \tau) = f(\zeta), \tag{3.2}$$

where c is a speed to be determined and $\zeta = \chi - c\tau$.

By substituting (3.2) into (3.1), we obtain a nonlinear ODE,

$$-cf' + 6ff' + f''' = 0. \tag{3.3}$$

We integrate (3.3) to obtain

$$-cf + f'' + 3f^2 = \alpha, \tag{3.4}$$

where α is an arbitrary constant of integration. We then multiply each side by $2f'$ and integrate again, to obtain

$$-cf^2 + (f')^2 + 2f^3 = 2\alpha f + \beta, \tag{3.5}$$

where β is another arbitrary constant of integration.

We are looking for a wave solution for which $f(\chi) \to 0, f'(\chi) \to 0$, and $f''(\chi) \to 0$ as $\chi \to \pm\infty$. In order for this to hold true in (3.4), $\alpha = 0$, and in (3.5), $\beta = 0$, which simplifies (3.5) to

$$-cf^2 + (f')^2 + 2f^3 = 0. \tag{3.6}$$

One can show that a solution to (3.6) is the soliton solution

$$f(\chi, \tau) = \frac{1}{2} c \operatorname{sech}^2[\frac{1}{2}\sqrt{c}(\chi - c\tau - \chi_0)]. \tag{3.7}$$

This solution corresponds to a dimensional water surface displacement of

$$f(x,t) = a_0 \operatorname{sech}^2[\sqrt{\frac{3a_0}{4h^3}}\left(x - c_0 t\left(1 + \frac{a_0}{2h}\right) - x_0\right)], \tag{3.8}$$

which is an isolated wave of arbitrary amplitude a_0, that travels to the right with speed $c_0\left(1 + \frac{a_0}{2h}\right)$. Here we see that allowing for weak nonlinearity increases the wave speed.

3.2 Fourier Transform Solutions of the KdV Equation

To gain insight into the effects of weak dispersion, we linearize (3.1) to obain

$$f_\tau + f_{\chi\chi\chi} = 0. \tag{3.9}$$

If we consider typical oscillatory waves of the form $f \sim e^{i(\omega\tau - k\chi)}$, then the corresponding nondimensional wave dispersion relation for (3.9) is

$$\omega = -k^3, \tag{3.10}$$

and the phase speed $c(k) = \frac{\omega}{k} = -k^2$. This value represents a correction to the linear (dimensional) phase speed of $c_0 = \sqrt{gh}$. So we see that dispersion slows down shallow water waves. The competing effects of nonlinearity and dispersion, which tend to increase and decrease the speed, respectively, are balanced in the soliton solution, thus allowing for the observation that was so surprising to J.S. Russell.

Following Hammack (1973), we can solve (3.9) using Fourier Transforms. To this end we represent $f(\chi, \tau)$ as

$$f(\chi, \tau) \int_{-\infty}^{\infty} A(k, \tau) e^{-ik\chi}\, dk = 0. \tag{3.11}$$

Then the Fourier Transform, $A(k,\tau)$, satisfies

$$\frac{\partial A}{\partial \tau} - ik^3 A = 0. \tag{3.12}$$

The solution for A is

$$\ln A = ik^3\tau + C, \tag{3.13}$$

which simplifies to

$$A(k,\tau) = A_0 e^{ik^3\tau}. \tag{3.14}$$

We can find the constant A_0 by taking the Fourier Transform of the initial conditions $f_0(\chi) := f(\chi, 0)$:

$$A_0(k) := A(k,0) = \int_{-\infty}^{\infty} f_0(\chi) e^{-ik\chi}\, d\chi. \tag{3.15}$$

This allows us to find the general solution for all times τ, by taking the inverse Fourier Transform. The general solution for a given $f_0(\chi)$ is

$$f(\chi,\tau) = \frac{1}{2\pi}\int_{-\infty}^{\infty} A_0(k) e^{(ik\chi + ik^3\tau)}\, dk. \tag{3.16}$$

3.3 Solutions of the Linearized KdV Equation for Two Initial Conditions

Here we consider two initial conditions relevant for tsunamis created by underwater earthquakes, using ideas from Hammack (1973) and Hammack & Segur (1974). The first corresponds to an upthrust, and the second to a downthrust. To obtain insight into the solutions, we consider the approximate solutions near the wave front and far from the wave front.

The first initial condition is a positive-displacement rectangular wave. This initial condition corresponds to

$$f_0(\chi) = \alpha[\mathcal{H}(\chi + 2\lambda) - \mathcal{H}(\chi)], \tag{3.17}$$

where $\mathcal{H}(\chi - \chi_0)$ is the Heavyside step function (see Kreyzig, 1999), defined as

$$\mathcal{H}(\chi - \chi_0) = \begin{cases} 1, \chi > \chi_0 \\ 0, \chi < \chi_0. \end{cases} \tag{3.18}$$

This is graphically represented by Figure 2.

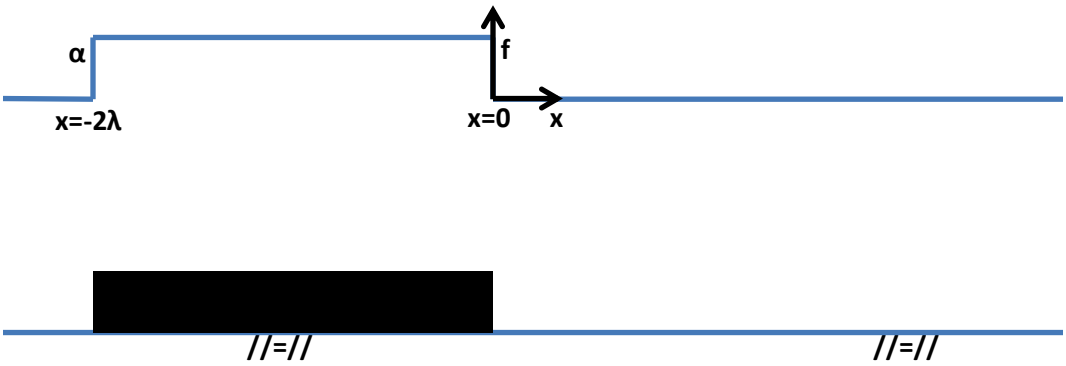

Figure 2: Schematic of initial condition (3.17)

We will use (3.17) and find its corresponding solution to the linearized KdV equation. We start by determining a value for $A_0(k)$. By substituting (3.17) into (3.15), we obtain

$$A_0(k) = \alpha \int_{-2\lambda}^{0} e^{-ik\chi}\, d\chi. \tag{3.19}$$

By evaluating the bounded integral in (3.19), we obtain

$$A_0(k) = \frac{i\alpha}{k}\left(1 - e^{ik(2\lambda)}\right). \tag{3.20}$$

We then factor (3.20) to obtain

$$A_0(k) = \frac{i\alpha}{k} e^{ik\lambda}\left(e^{-ik\lambda} - e^{ik\lambda}\right), \tag{3.21}$$

which simplifies to

$$A_0(k) = \frac{2\alpha}{k} e^{ik\lambda} \sin k\lambda. \tag{3.22}$$

Therefore, the solution for all times τ for the initial condition (3.17) is

$$f(\chi, \tau) = \frac{\alpha}{\pi} \int_{-\infty}^{\infty} \frac{\sin k\lambda}{k} e^{i(k\chi + k^3\tau + k\lambda)}\, dk. \tag{3.23}$$

The second initial condition we will consider is for a negative-displacement rectangular wave. This initial condition corresponds to

$$f_0(\chi) = \alpha[\mathcal{H}(\chi) - \mathcal{H}(\chi + 2\lambda)]. \tag{3.24}$$

Visually, (3.24) is represented by Figure 3.

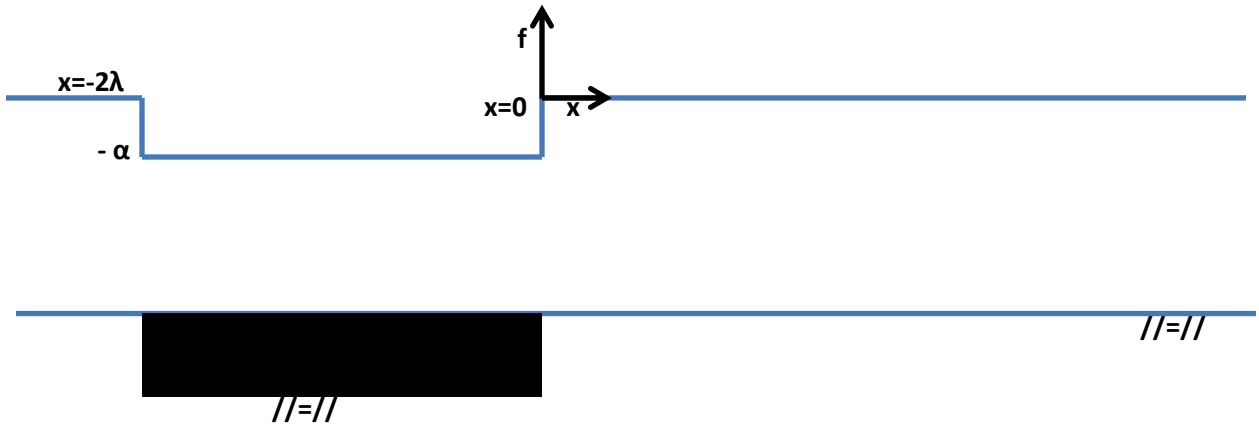

Figure 3: Initial condition for (3.24)

We follow the same method as in the previous case. We note that the formula for $f_0(\chi)$ in (3.24) is simply the formula in (3.21) multiplied by -1. The result differs by a minus sign only, so here,

$$f(\chi,\tau) = \frac{-\alpha}{\pi}\int_{-\infty}^{\infty} \frac{\sin k\lambda}{k} e^{i(k\chi+k^3\tau+k\lambda)}\, dk. \tag{3.25}$$

3.4 Asymptotic Behavior and Long-Time Solutions

While (3.23) and (3.25) are exact solutions for the initial conditions, it is difficult to see the behavior of the wave surface displacement based upon these integrals. Therefore, we study the behavior of the waves for large times ($\tau \to \infty$) in two areas: near the wave front, for which $\chi \approx 0$, and far away from the wave front, for which $\chi \to \infty$.

3.4.1 Behavior Near the Wave Front

Recall that we have allowed for weak dispersion, so that wave speeds depend on wavelength. The fastest waves have $k \to 0$, so these are the waves that will be at the wave front for large times. For the area near the wave front, we look at waves for which $k \approx 0$. For convenience, define the similarity variables, ξ and κ, as

$$\xi = \frac{\chi}{(3\tau)^{1/3}}, \kappa = (3\tau)^{1/3}k. \tag{3.26}$$

For arbitrary initial data, consider (3.16) in terms of the new variables (3.26), to find

$$f(\xi,\tau) = \frac{(3\tau)^{-1/3}}{2\pi}\int_{-\infty}^{\infty} A_0\left[\frac{\kappa}{(3\tau)^{1/3}}\right] e^{i(\kappa\xi+\frac{1}{3}\kappa^3)} d\kappa. \tag{3.27}$$

We are interested in τ large and $k \sim 0$, which implies that $\kappa \sim 0$, if we can control τ. The analysis will tell us how large τ must be for the asymptotics to be a valid description of the behavior. We approximate $A_0(k)$ using a Taylor series expansion about $k = 0$. This approximation yields

$$A_0(k) \sim A_0(0) + kA_0'(0) + k^2 A_0''(0) + \cdots \tag{3.28}$$

By using (3.28) and (3.26), (3.27) becomes

$$\begin{aligned} f(\chi,\tau) = \frac{1}{(3\tau)^{1/3}} \Bigg\{ & A_0(0)\frac{1}{2\pi}\int_{-\infty}^{\infty} e^{i\left(\kappa\xi+\frac{1}{3}\kappa^3\right)} d\kappa \\ & + \frac{A_0'(0)}{(3\tau)^{1/3}}\frac{1}{2\pi}\int_{-\infty}^{\infty} \kappa e^{i\left(\kappa\xi+\frac{1}{3}\kappa^3\right)} d\kappa \\ & + \frac{A_0''(0)}{2(3\tau)^{2/3}}\frac{1}{2\pi}\int_{-\infty}^{\infty} \kappa^2 e^{i\left(\kappa\xi+\frac{1}{3}\kappa^3\right)} d\kappa + \cdots \Bigg\}. \end{aligned} \tag{3.29}$$

Equation (3.29) can be rewritten in terms of the Airy function:

$$Ai(\xi) = \frac{1}{2\pi}\int_{-\infty}^{\infty} e^{i\left(\kappa\xi+\frac{1}{3}\kappa^3\right)} d\kappa, \tag{3.30}$$

so that (3.29) simplifies to

$$\begin{aligned} f(\chi,\tau) = & \frac{A_0(0)}{(3\tau)^{1/3}} Ai(\xi) + \frac{A_0'(0)}{i(3\tau)^{2/3}} Ai'(\xi) - \frac{A_0''(0)}{2(3\tau)} Ai''(\xi) \\ & + \mathcal{O}\left(\frac{1}{(3\tau)^{4/3}}\right). \end{aligned} \tag{3.31}$$

A graph of the Airy function is shown in Figure 4.

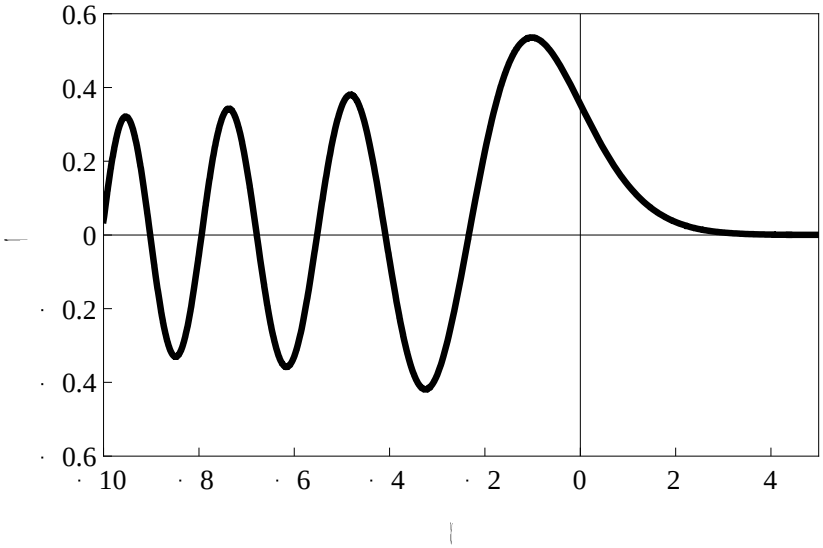

Figure 4 – A graph of the Airy Function $Ai(\chi)$ for $\chi \in [-10,5]$

We define three constants V, M_1, M_2 as

$$V = A_0(0), \tag{3.32}$$

$$M_1 = iA_0'(0), \tag{3.33}$$

and

$$M_2 = -A_0''(0), \tag{3.34}$$

where V measures the volume of the initial displacement, and M_1 and M_2 are wave moments.

In terms of these parameters, (3.31) becomes

$$f(\xi,\tau)=\frac{V}{(3\tau)^{1/3}}Ai(\xi)-\frac{M_1}{(3\tau)^{2/3}}Ai'(\xi)+\frac{\frac{1}{2}M_2}{(3\tau)}Ai''(\xi)+\mathcal{O}\left[\frac{1}{(3\tau)^{4/3}}\right]. \tag{3.35}$$

For the positive initial data (3.17), (3.35) becomes

$$f(\xi,\tau)=\frac{2\alpha\lambda}{(3\tau)^{1/3}}\left[Ai(\xi)+\frac{\lambda}{(3\tau)^{1/3}}Ai'(\xi)-\frac{\frac{2}{3}\lambda^2}{(3\tau)^{2/3}}Ai''(\xi)+\cdots\right]. \tag{3.36}$$

A graph of (3.36) for a constant time τ is shown in Figure 5.

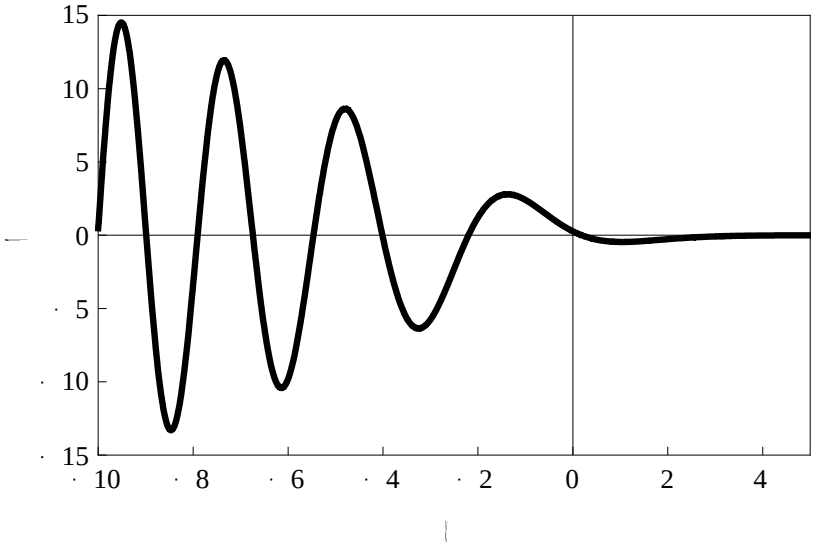

Figure 5 – Graph of Equation (3.36)

For the initial negative initial data (3.24), (3.35) becomes

$$f(\xi,\tau)=\frac{-2\alpha\lambda}{(3\tau)^{1/3}}\left[Ai(\xi)+\frac{\lambda}{(3\tau)^{1/3}}Ai'(\xi)-\frac{\frac{2}{3}\lambda^2}{(3\tau)^{2/3}}Ai''(\xi)+\cdots\right]. \tag{3.37}$$

A graph of (3.37) is shown in Figure 6.

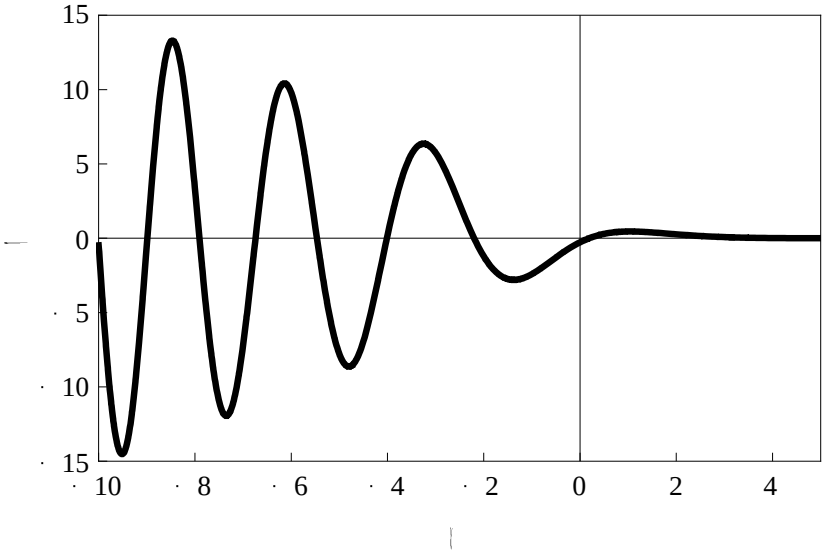

Figure 6 – Graph of Equation (3.37)

The long-time condition states that (3.35) only holds as a solution to the KdV equation when each succeeding term in the expression decreases in magnitude, so that it becomes asymptotic as $\tau \to \infty$.

The Airy functions and their derivatives are all order 1, so we require that

$$\left|\frac{\frac{1}{2}M_2}{(3\tau)}\right| \ll \left|\frac{M_1}{(3\tau)^{2/3}}\right| \ll \left|\frac{V}{(3\tau)^{1/3}}\right|. \tag{3.38}$$

There are two conditions that we place on (3.38). First, we consider only data for which $V \neq 0$; if $V = 0$, the solution is zero for all time and space. Next, we also note that we can always find a coordinate system for which $M_1 = 0$ when $V \neq 0$. Therefore, (3.38) becomes

$$\left|\frac{\frac{1}{2}M_2}{(3\tau)}\right| \ll \left|\frac{V}{(3\tau)^{1/3}}\right|. \tag{3.39}$$

Solving (3.39) for τ, we obtain

$$\tau \gg \frac{1}{3}\left|\frac{M_2}{2V}\right|^{3/2}. \tag{3.40}$$

For the initial condition (3.17), this simplifies to

$$\tau \gg \frac{2}{9}\sqrt{\frac{2}{3}}\lambda^3. \tag{3.41}$$

We will use these theoretical results as a framework for looking at recent tsunamis in Sections 4 and 5.

3.4.2 Behavior Far from the Wave Front

In order to determine the behavior of the waves far from the wave front, we will use a method called Stationary Phase, developed by Lord Kelvin. Here we follow Stoker (1957). Recall that we found an exact solution for the wave behavior in (3.16), which applies for all times and for all initial data. We can rewrite (3.16) as

$$f(\chi,\tau)=\frac{1}{2\pi}\int_{-\infty}^{\infty}A_0(k)e^{ig(k)\tau}\,dk, \tag{3.42}$$

where

$$g(k)=k\left(\frac{\chi}{\tau}\right)+k^3=k\left(\frac{\chi}{t}\right)-W(k). \tag{3.43}$$

We define (3.43) as the wave phase function.

In examining the behavior far from the wave front, we are looking for waves with a specific wave number. We did this for waves at the wave front by choosing waves for which $k\sim 0$. In order to do this for trailing waves we must have

$$\frac{\chi}{\tau}=c_g, \tag{3.44}$$

where c_g represents the group velocity of the wave number that we choose. Again, we are examining the behavior for long times τ; in this case, we approximate (3.42) for $\tau\to\infty$ and fixed $\frac{\chi}{\tau}$.

We can find the extrema of the wave phase function $g(k)$ by finding values of k for which $g'(k)=0$. These points k_0 occur when

$$g'(k_0)=\frac{\chi}{\tau}+3k_0^2=0. \tag{3.45}$$

This implies that (the nondimensional wave number) $k_0=\pm\left(-\frac{\chi}{3\tau}\right)^{1/2}$. These points are called the stationary points. If we choose $\frac{\chi}{3\tau}<0$, then we will be examining a wave that is trailing the wave front, because its group speed will be less than the speed of our reference frame (traveling with the wave front), $\sqrt{gh}$. For example, we can choose $\frac{\chi}{3\tau}=-16$, which would imply that $k_0=\pm 4$. By looking at the second derivative of the wave phase function, we find that $g''(4)=24$, so this extremum is a minimum point for the wave phase $g(k)=-48k+k^3$.

We can approximate the integrand of (3.42) by a Taylor series expansion of $g(k)$ about $k=k_0$, because the nonzero contribution to the integral (3.42) comes from these points. By doing this expansion, we obtain

$$g(k)=g(k_0)+(k-k_0)g'(k_0)+\frac{1}{2}(k-k_0)^2g''(k_0)+\cdots \tag{3.46}$$

However, since k_0 is an extremum of $g(k)$, $g'(k_0)=0$. Therefore, if $g''(k_0)\neq 0$, we obtain

$$g(k) - g(k_0) \sim \frac{1}{2}(k - k_0)^2 g''(k_0). \tag{3.47}$$

Taking $A_0(k) \sim A_0(k_0)$, we can rewrite (3.42) as the contribution to $f(\chi, \tau)$ near k_0, represented as

$$f(\chi, \tau) = \frac{1}{2\pi} A_0(k_0) e^{ig(k_0)\tau} \int_{-\infty}^{\infty} e^{i\frac{1}{2}(k-k_0)^2 g''(k_0)\tau}\, dk. \tag{3.48}$$

We define a substitution variable $v^2 = g(k) - g(k_0)$. Then, $v \sim (k - k_0)\sqrt{\frac{1}{2}g''(k_0)}$, and $dv = dk\sqrt{\frac{g''(k_0)}{2}}$. With this substitution, the integral in (3.48) becomes $\int_{-\infty}^{\infty} e^{i\tau v^2} dv$. One can solve this integral by transforming it to the error integral (erf) and using integration in the complex plane. By doing this, (3.48) becomes

$$f(\chi, \tau) = \frac{1}{2\pi} A_0(k_0) \left[\frac{2\pi}{\tau |g''(k_0)|}\right]^{1/2} e^{i[g(k_0)\tau \pm \frac{\pi}{4}]}. \tag{3.49}$$

We choose $+\frac{\pi}{4}$ when $g''(k_0) > 0$ and $-\frac{\pi}{4}$ when $g''(k_0) < 0$. Equation (3.49) represents the contribution to the wave amplitude from a single stationary point. If there are multiple stationary points, as there are in our case, we must sum the contribution of each stationary point. The result of this sum when $g''(k_0) \neq 0$, for N stationary points is

$$f(\chi, \tau) \sim \frac{1}{2\pi} \sum_{n=1}^{N} A_0(k_{0n}) \sqrt{\frac{2\pi}{\tau |W''(k_{0n})|}}\, e^{i[k_{0n}\chi - W(k_{0n})\tau \pm \frac{\pi}{4}]}. \tag{3.50}$$

If $g''(k_0) = 0$, then we must extend the Taylor series into higher order terms.

Using our initial conditions from (3.22) and (3.50), we obtain

$$f(\chi, \tau) \sim \frac{2\alpha}{\sqrt{3\pi\tau}} \frac{\sin k_0\lambda}{k_0^{3/2}} \cos\theta\,, \theta = k_0\chi + {k_0}^3\tau + \frac{\pi}{4} + k_0\lambda, \tag{3.51}$$

where 2λ is the width of the initial displacement.

Therefore, the trailing waves are rapid oscillations, governed by an envelope function,

$$E(k_0) = \frac{2\alpha}{\sqrt{\pi}} \frac{1}{\sqrt{3\tau}} \frac{\sin k_0\lambda}{k_0^{3/2}}. \tag{3.52}$$

This envelope function creates groups of waves. The nodes of the wave groups correspond to the zeros of (3.52):

$$\sin k_0\lambda = 0 \text{ or } k_0\lambda = n\pi, n \in \mathbb{N}. \tag{3.53}$$

The maxima of the envelope occur approximately midway between two consecutive nodes, so that

$$k_0\lambda \approx (2n+1)\frac{\pi}{2}, n \in \mathbb{N}. \tag{3.54}$$

The amplitude at these maxima is given as

$$|E|_{max} = \frac{2\alpha}{\sqrt{\pi}}\frac{1}{\sqrt{3\tau}}\frac{1}{k_0^{3/2}}. \tag{3.55}$$

4. Experimental Simulations

Here we use Sections 2 and 3 as a theoretical framework for laboratory experiments in the William G. Pritchard Fluid Mechanics Laboratory. In order to qualitatively observe these solutions, we conducted laboratory experiments in order to observe both solitons and the Airy functions created by the nonlinear, dispersive KdV equation. We performed these experiments in a wave tank that measured 50 feet long, 10 inches wide, and at a water depth of 5.0 cm, or approximately 2 in. Two sets of experiments were run: the first set involved various solitons and the second involved several sets of initial conditions similar to Figures 2 and 3. Eight separate experiments are described below.

For each experiment, data were measured four pressure transducers along the bottom of the tank. Each of these gauges recorded the pressure of the water at the transducer at a sampling rate of 500 Hz for a time of 30 s. We can convert these pressure measurements into surface amplitude measurements, which allow us to determine the wave behavior at the surface. The pressure transducers take the water pressure and output a voltage to the computer, where it is digitized and recorded using LabView software and NI hardware. The transducers were calibrated by filling the tank to a series of known water depths in 1 cm increments and measuring the output voltage from each gauge at each depth. When the output voltage is graphed as a function of water depth, the slope of the line gives us a relationship between output voltage from the gauges and the depth of the water at the transducer. We compute the surface data from the pressure data using

$$\eta(x_j,t) = p_j(t) - \frac{h^2}{2c^2}\frac{d^2p_j(t)}{dt^2} + \frac{h^4}{24c^4}\frac{d^4p_j(t)}{dt^4} - \frac{h}{c^2}\frac{d^2p_j(t)}{dt^2} - \frac{h}{c^2}\frac{dp_j(t)}{dt}, \qquad (4.1)$$

where $j = 1,2,3,4$, $x_j = 170, 474.8, 779.6, 1084.4$ cm, and c is the measured speed of the wave. To implement (4.1), we took fast Fourier Transforms of the pressure time series and the inverse Transform to obtain $p_j = f(t)$, where p_j represents the pressure at the j^{th} gauge. Then, we took the derivatives of $f(t)$ to use in (4.1). We measured c by finding the time it took for the peak of the first wave to travel between two transducers. The inversion (4.1) was developed by Vishal Vasan (gradute student, University of Washington, private communication).

We describe the wave generation for eight different experiments below.

4.1 Forward Soliton: $a_0 = 2$ cm

We programmed Equation (3.8) with $a_0 = 2$ cm and $h = 5$ cm into the computer in order to generate a soliton with an amplitude of 2 cm. The program actually output velocities scaled such that $u_0 = \frac{a_0 c_0}{h}$. The wave paddle was a vertical plate attached to a motor-driven belt, which received a digitized time series of velocities from the program. The soliton propagated in the direction of the pressure gauges, which we will refer to as the "forward" direction.

The measured data are shown in Figure 7. The left column shows the data for the entire time interval of 30 s for each gauge. During this time, the soliton reflected off the back wall. The reflected wave is

visible in the last three rows of Figure 7. The right column is a zoomed portion of the first peak of the data.

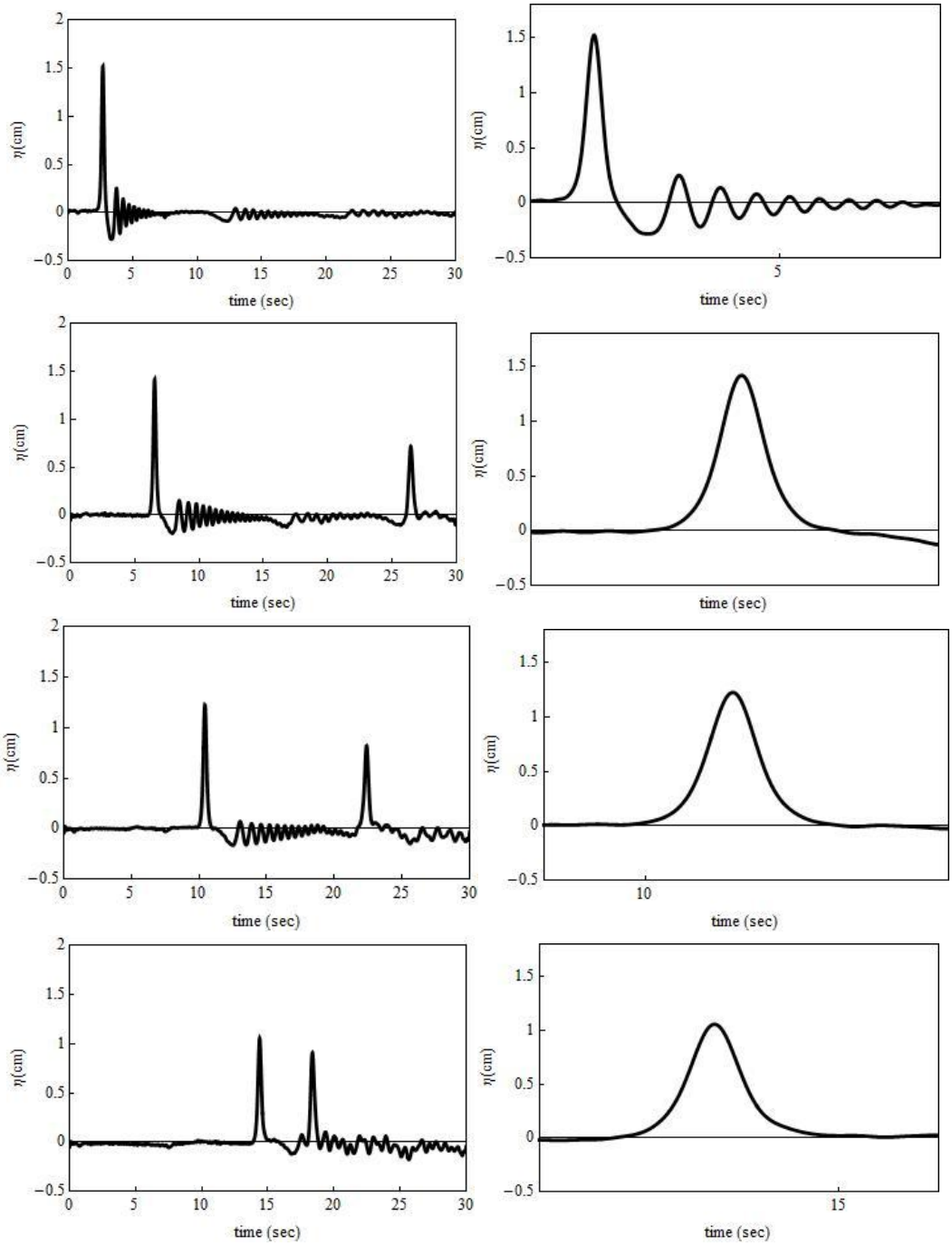

Figure 7 – Data from Experiment 1

When we zoom in on the first peak that each gauge records, we find a shape similar to a soliton shape. A comparison between the recorded data and a true soliton is shown in Figure 8. The data are marked with a solid line, while the theoretical soliton is marked with a dashed line.

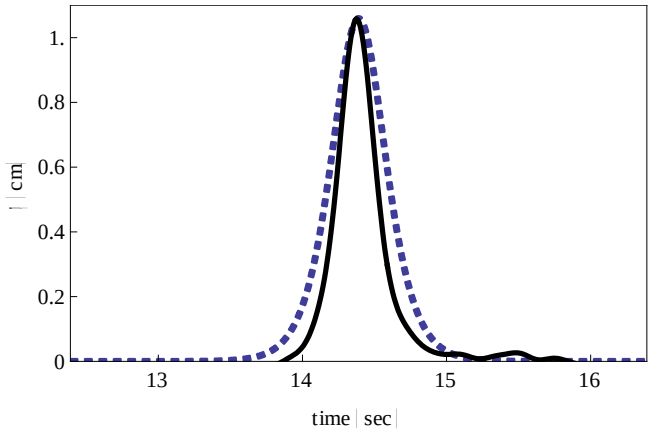

Figure 8 – Comparison between Measured Data and Theoretical Prediction

We see that our measured data is in qualitative agreement with a soliton. The gaps between the measured data and the theoretical predictions come about as a result of viscous properties of the water, which we neglected in our theoretical predictions. These viscous properties cause the wave's energy to decay over time, unlike a theoretical inviscid soliton, which does not decay.

The speed of the wave was also measured from the data. The speed of the wave from each experiment, along with the ratio of amplitudes from the first to the fourth gauge, is shown in Table 1.

Experiment	$a_0(x_1)$ (cm)	$\frac{a_0(x_4)}{a_0(x_1)}$	c (cm/s)
1	1.22	0.766	78.0
2	1.562	0.767	80.4
3	-0.46	0.445	65.9
4	-0.514	0.470	65.4
5	1.544	0.834	80.7
6	-0.46	0.366	66.3
7	1.284	0.862	79.7
8	1.726	0.848	82.4

Table 1 – Measured Amplitude Ratios and Speeds

In all of our experiments, we observed that the amplitude of the waves decayed as they propagated. This is also due to the viscous effects of the water, which were neglected in our predictions. These viscous effects were most readily observed in Experiments 3, 4, and 6, where there was a negative initial displacement. If there were no viscous effects, then the waves would propagate without a loss of amplitude or energy, as our theoretical framework predicts. However, these viscous effects cause some decay in the amplitude and the energy of the waves.

We also see that a small radiative tail evolves, which is not included in (3.8). This imperfection is a perturbation brough about by the wavemaker motion. Finally, the amplitude of the soliton decays during evolution due to viscous effects, which are neglected in the theory.

This soliton is very similar to the "wave of translation" that J.S. Russell observed. The wave did not disperse into a train of waves, but rather, it maintained its shape as it propagated. This is what we expected to occur based on (3.8).

4.2 Forward Soliton $a_0 = 3$ cm

For this experiment, we used the same procedure as Section 4.1, but the generated soliton used $a_0 = 3$ cm. Again, the soliton propagated in the direction of the pressure gauges. Much like in experiment 1, the wave reflected off the back wall of the tank – these reflections can be seen in the last three rows of Figure 9.

The measured data for this experiment are shown in Figure 9.

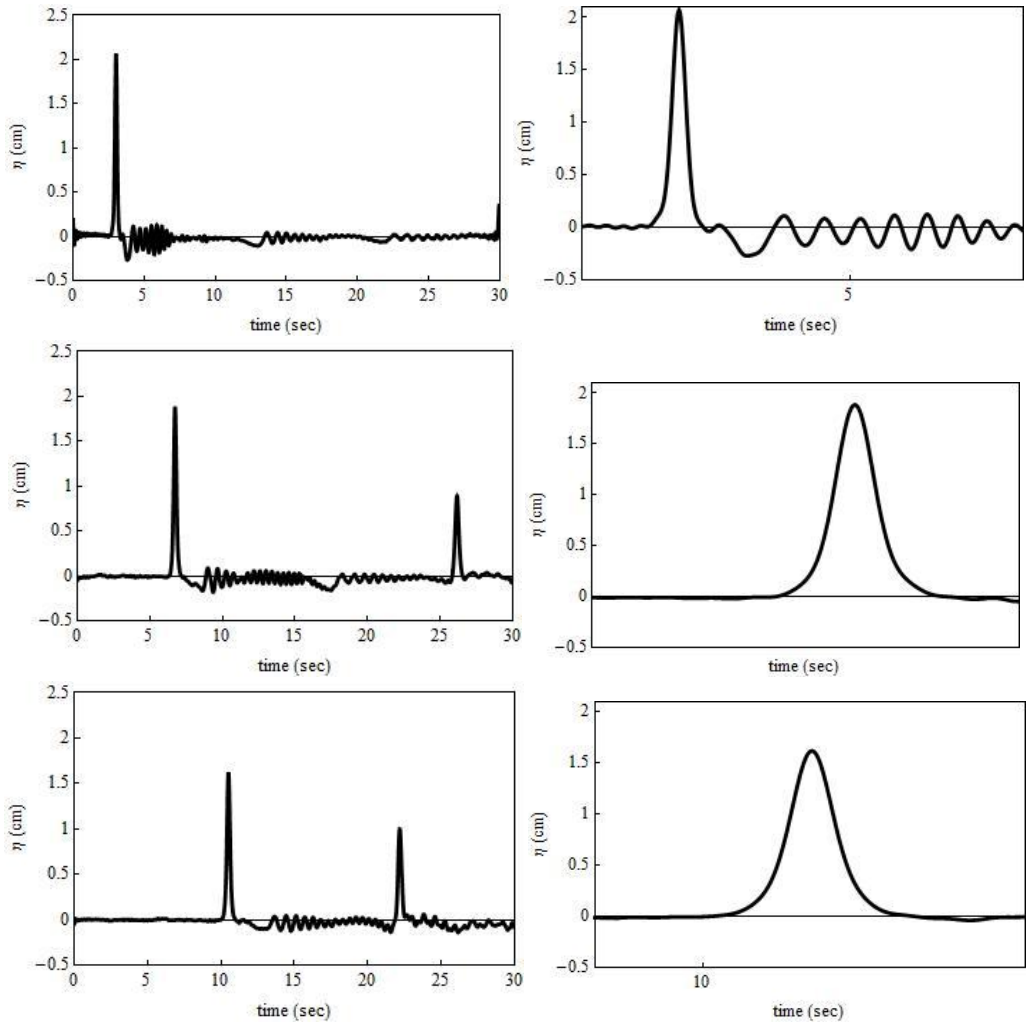

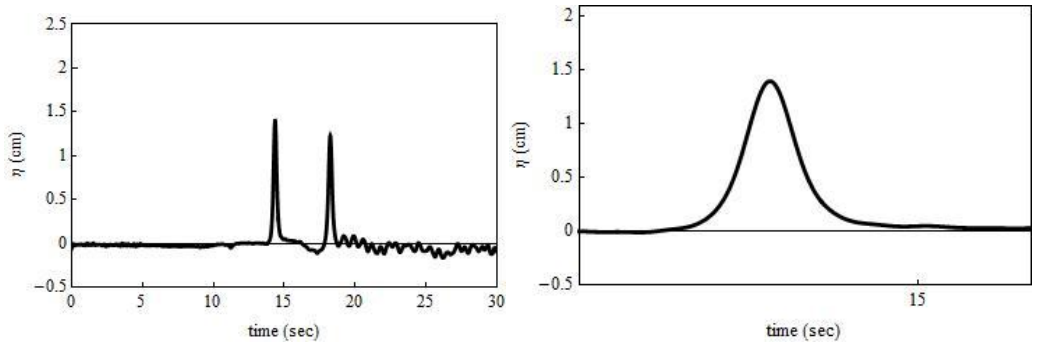

Figure 9 – Data from Experiment 2

Again, we observe a soliton waveform propagating along the tank. A comparison between the data collected and the predicted soliton form is shown in Figure 10.

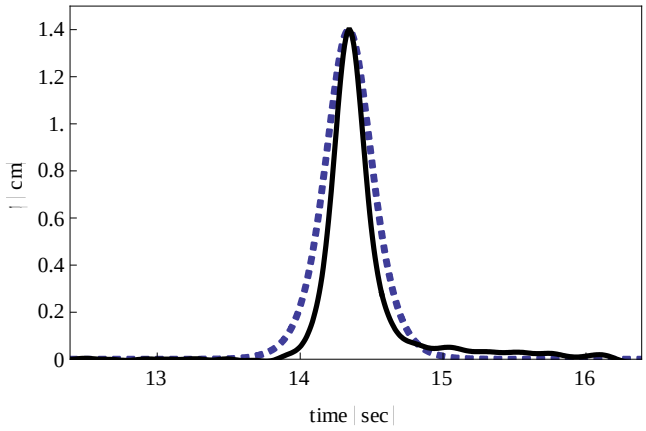

Figure 10 – Comparison between Measured Data and Prediction

Again, this wave is in qualitative agreement of a soliton, with the exception of the gaps caused by the viscous effects of the water. These gaps appear to be similar in size to those seen in Figure 8. This is to be expected, because we see in Table 1 that the waves in Experiments 1 and 2 decayed in amplitude by almost exactly the same ratio. Therefore, it makes sense that they would decay by the same amount of energy by the viscous effects.

We can also see that the amplitude of the wave at the first gauge and the speed were greater in this experiment than in Experiment 1. This is as we expect, because the initial wave had a greater amplitude in this experiment, and the speed of a soliton is directly proportional to its amplitude. Therefore, solitons with a greater amplitude also have greater propagation speeds.

4.3 Reverse Soliton: $a_0 = 2$ cm

For this experiment, we again used the same procedure as the previous two experiments. However, we changed the program so that the soliton propagated away from the pressure gauges. This created a depression that propagated towards the pressure gauges, which we were able to measure. The soliton generated had an amplitude of 2 cm.

The measured data for this experiment are shown in Figure 11.

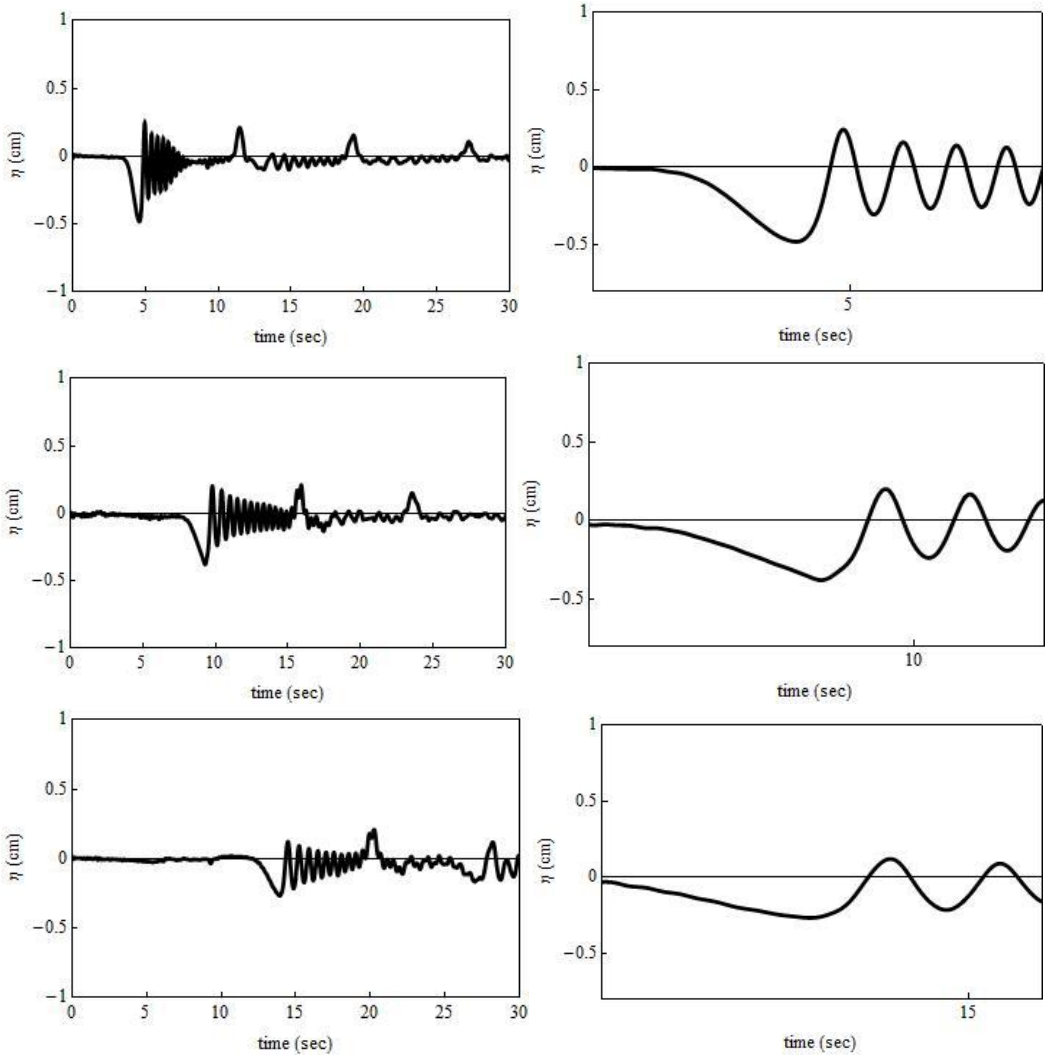

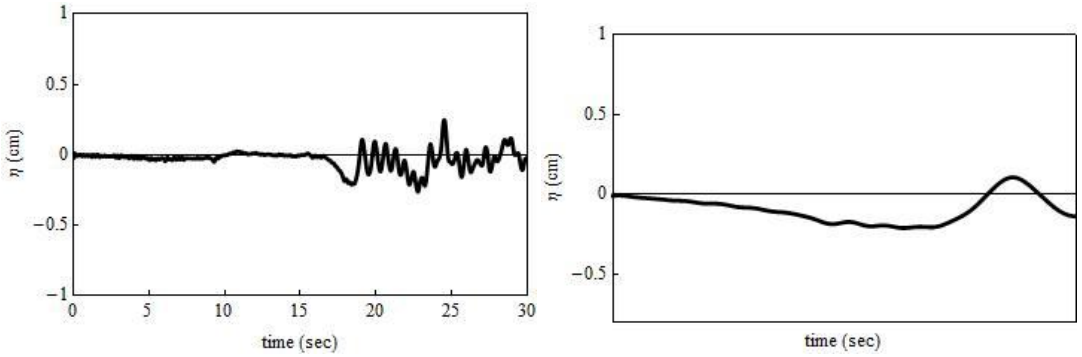

Figure 11 – Data from Experiment 3

The secondary peaks in the first row at approximate times 12, 18, and 26 seconds are reflections from some of the water from the initial soliton propagation slipping past the plate.

In this experiment, the depression of water propagated along the tank opposite the direction of the soliton (i.e. in the direction of the pressure gauges). This depression behaved much like the Airy function shown in Figure 6,starting with a large negative amplitude that decreased in time at a fixed x. While not a rectangular wave, this initial condition is similar to that of (3.24) in that they are both negative volume displacements.

4.4 Reverse Soliton: $a_0 = 3$ cm

For this experiment, we used the same procedure as section 4.3, but the generated soliton had $a_0 = 3$ cm. Again, the soliton propagated away from the pressure gauges, creating an initial negative volume displacement.

The measured data for this experiment are shown in Figure 12.

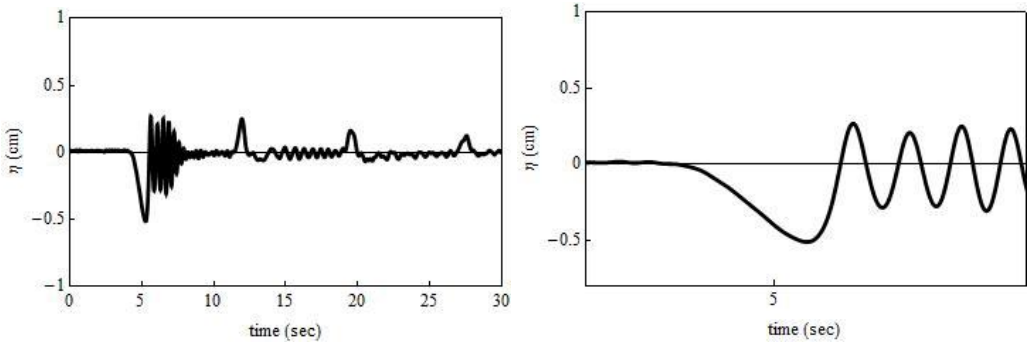

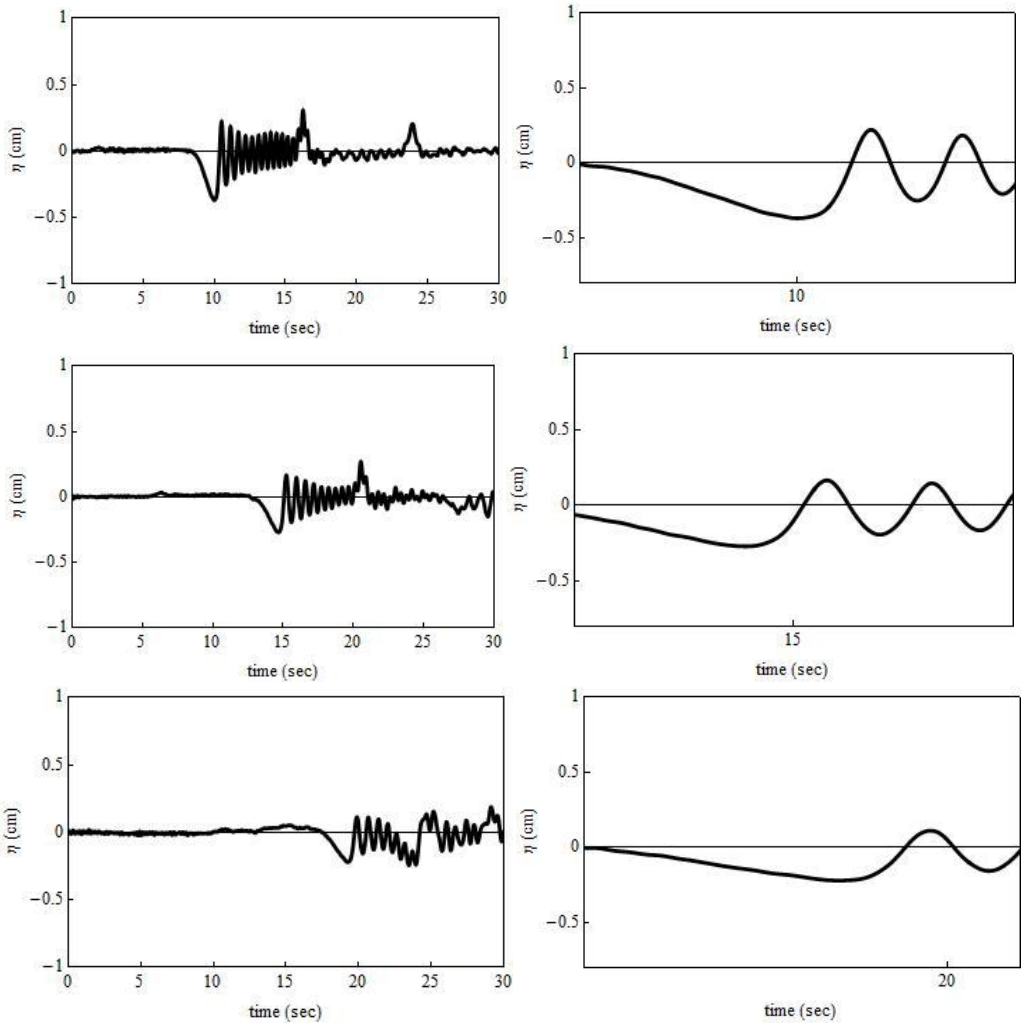

Figure 12 – Data from Experiment 4

Much like in Experiment 3, creating a soliton propagating away from the gauges causes a wave depression to propagate in the direction of the gauges. This depression has a slightly larger initial amplitude, which is to be expected, as the initial soliton had a larger amplitude. Again, as in experiment 3, the amplitude of the depression decreased over time for a constant x, as the Airy function does. This again shows that the leading depression wave is consistent with an Airy function representation, as shown in Figure 6.

4.5 Wave Generation by Plate Depression

For this experiment, we took a rigid teflon plate, 35 cm long and 20 cm wide, and created waves by pushing it from the surface to the bottom of the tank. We placed the center of the plate at the same place the soliton-generating plate was placed in the previous experiments. By doing this, the distance between the waves and the gauges remain the same as in Experiments 1 to 4.

The data that we measured for this experiment are shown in Figure 13. The reflected waves are seen in rows 3 and 4.

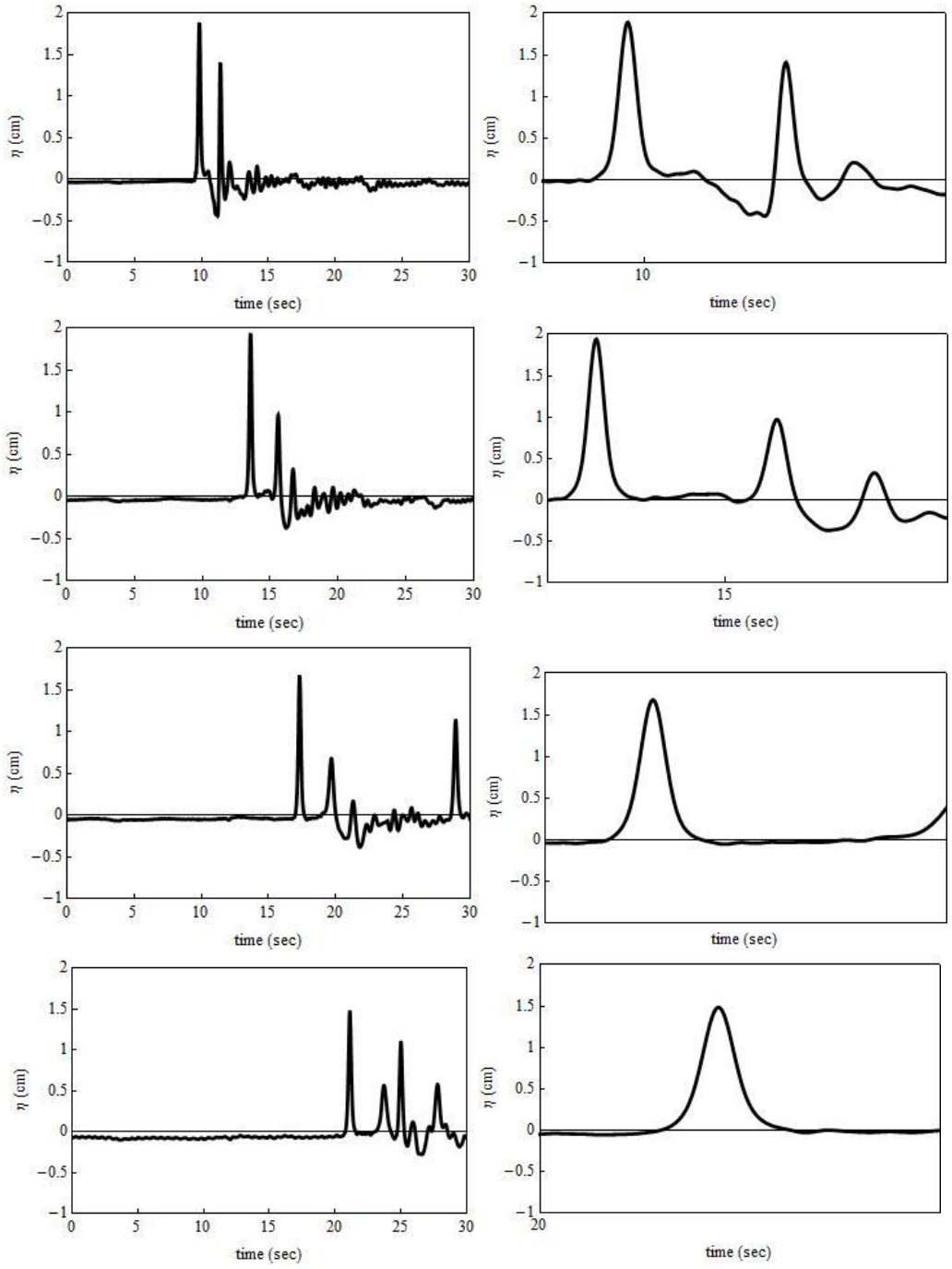

Figure 13 – Data from Experiment 5

It appears that performing this action with the plate generated waves similar to those generated by the initial conditions in (3.17). The first few leading peaks resemble an Airy function, like that in Figure 4, as the subsequent peaks decrease in amplitude. These peaks are followed by rapid oscillations similar to

what theory predicts in the trailing wave region. However, another explanation for the two or three leading peaks is that they are individual soliton solutions to (3.1). A theoretical framework for this possibility is provided by using a nonlinear transform, such as the inverse scattering transform, as discussed in Ablowitz and Segur (1981).

It seems that by pushing the plate downwards from the surface, the water near the plate was forced upwards, much like the rectangular wave in (3.17). Therefore, it would make sense that this creates similar waves to what theory predicts the rectangular wave evolves into.

4.6 Wave Generation by Plate Uplift

This experiment had a similar procedure to Experiment 5. However, instead of pushing the plate from the surface to the bottom of the tank, we started with the plate on the bottom of the tank and quickly pulled it, in one motion, to the surface of the water. We used the same plate as Experiment 5, and placed it in the same location.

The data from this experiment are shown in Figure 14.

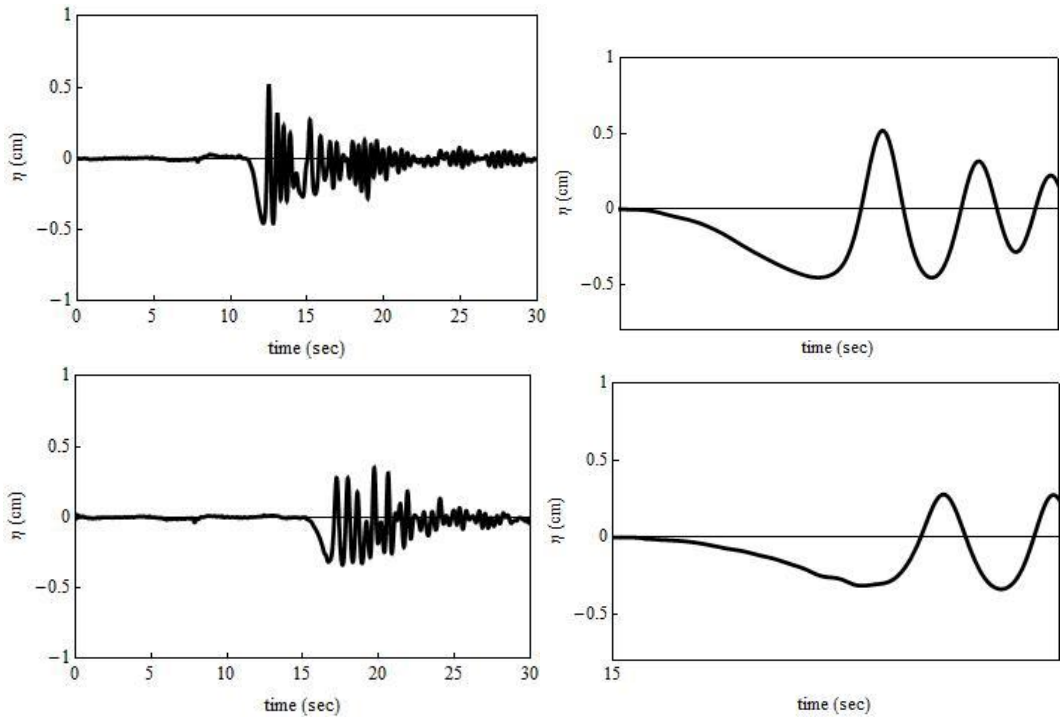

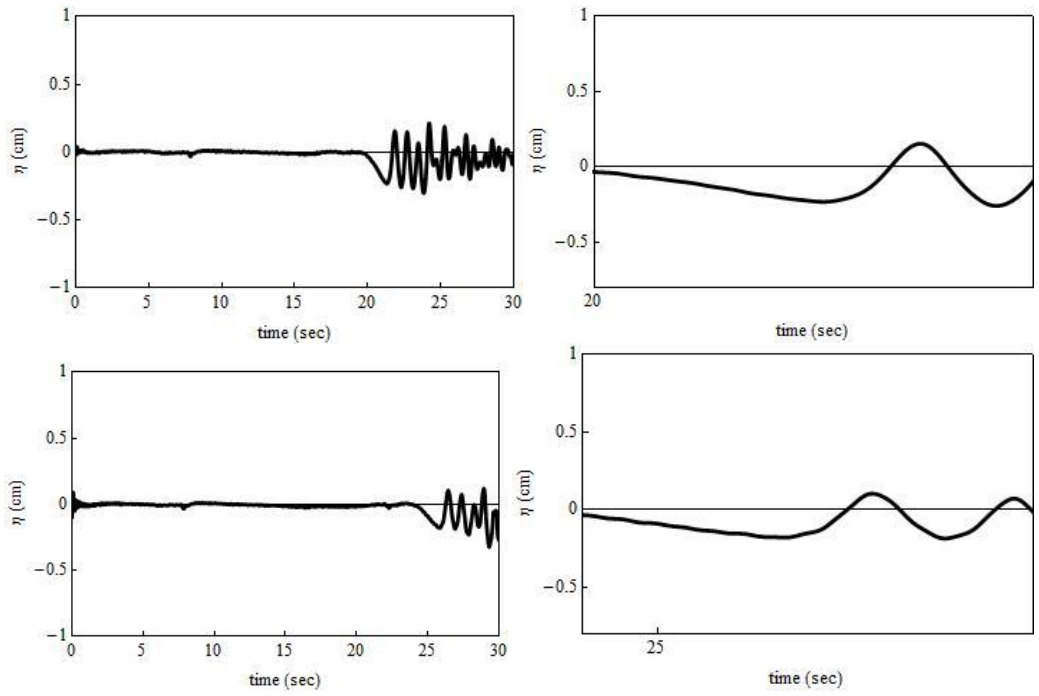

Figure 14 – Data from Experiment 6

Much like how Experiment 5 mirrors the initial conditions from (3.17), this experiment seems to resemble the conditions in (3.24) of a negative rectangular wave. This experiment produced a leading depression, much like an Airy function created by a negative rectangular wave, as seen in Figure 6. Again, as expected with the solution (3.31), the amplitude of this depression decreases as the wave propagates. Behind this depression front is a region of rapid oscillations, as expected from the trailing wave region.

Much like pushing the plate to the bottom of the tank caused the nearby water levels to elevate like a positive rectangular wave, pulling the plate from the bottom of the tank causes a depression that propagates like a negative rectangular wave. This explains how the wave's surface behavior is similar to the wave behavior that evolves from (3.24).

4.7 Wave Generation by Plate Sliding

In this experiment, we used the same plate as Experiments 5 and 6 and placed it at the same location as the previous experiments. Rather than manipulating the height of the plate, we placed the plate at the bottom of the tank, then quickly slid it forward 50 cm along the bottom. This "slip" motion is another qualitative motion that can occur in an earthquake.

The measured data are shown in Figure 15.

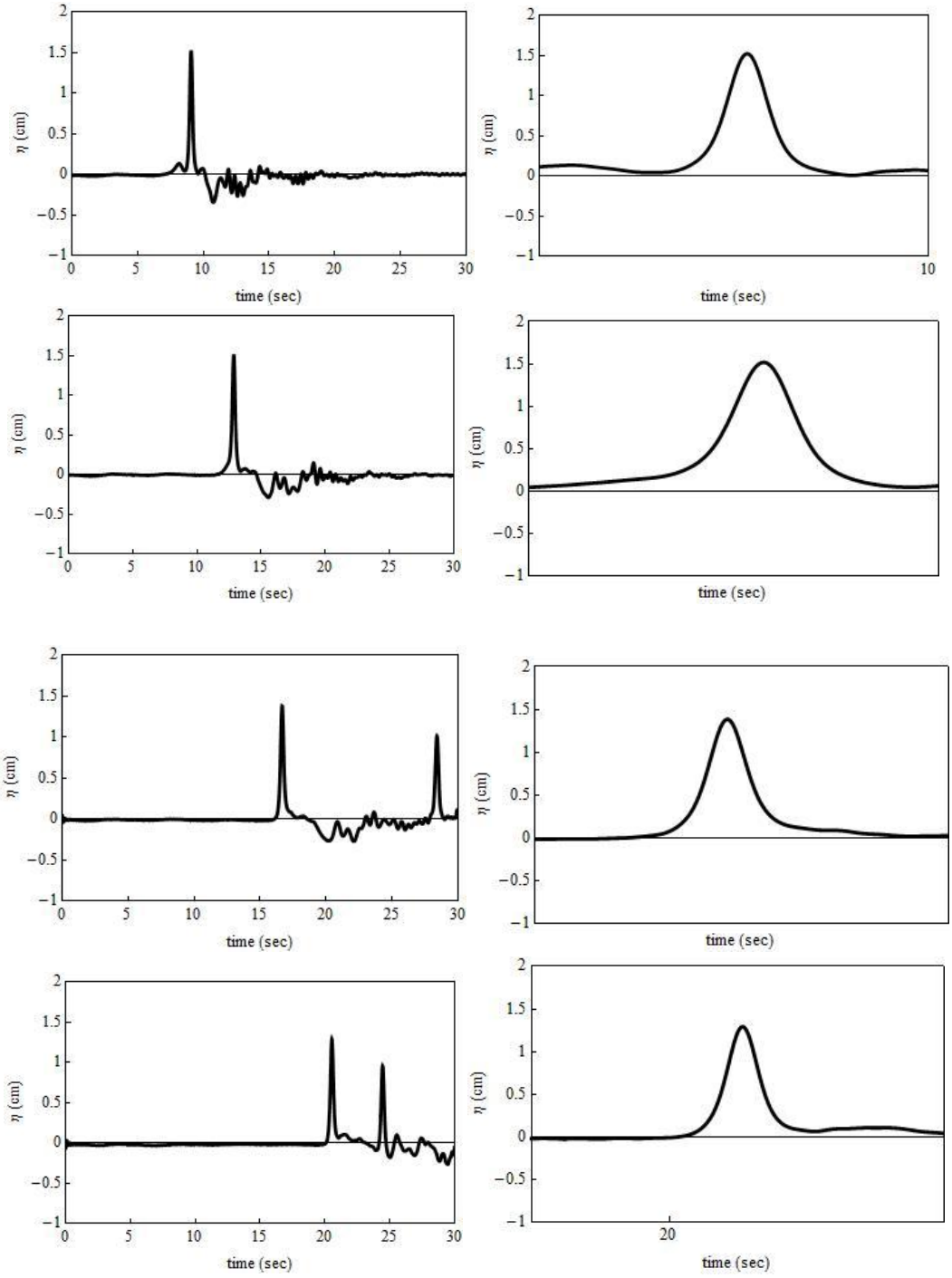

Figure 15 – Data from Experiment 7

The data we measured shows a leading peak followed by very little to no oscillations. By zooming in on this first peak, it appears that this peak is similar to a soliton propagating in the direction of the gauges. A comparison between this observed wave and a theoretical soliton is shown in Figure 16.

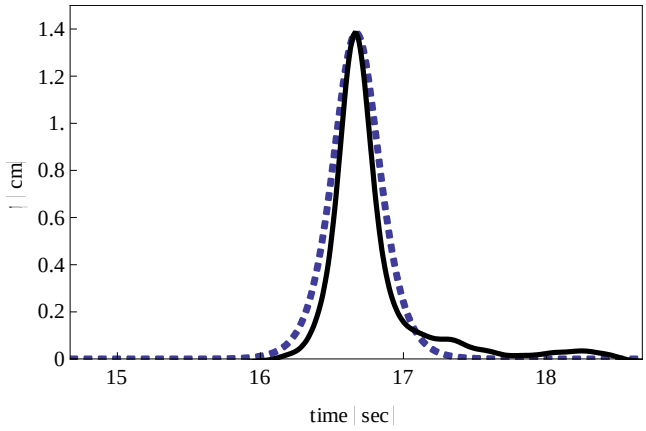

Figure 16 – Comparison of Measured Data and Prediction

This wave is also in qualitative agreement with a soliton. Again we see the gaps caused by the energy decay, as a result of viscous effects. However, these gaps are not as large as those in Experiments 1 and 2. This is because the viscous properties seemed to have less effect in this experiment, as exhibited by the ratio of decay. For this experiment, the decay ratio was 0.862, while the ratio for Experiments 1 and 2 was approximately 0.766, meaning the viscous properties had more of an effect on the waves in Experiments 1 and 2.

This experiment also shows how the speed of a soliton depends on its amplitude. This soliton had an initial amplitude in between that of Experiments 1 and 2, as seen in Table 1. Its speed also lies between the measured speeds from Experiments 1 and 2. This is as expected from (3.8), which shows that the speed is directly proportional to the amplitude – larger amplitudes cause larger speeds.

4.8 Wave Generation by Plate Sloping

In this experiment, we started with the plate on the bottom of the tank. Then, we lifted the end of the plate furthest from the gauges to the surface, while leaving the other end on the bottom. This created waves propagating in the direction of the gauges, and provides another qualitative type of earthquake motion.

The data from this experiment is shown in Figure 17.

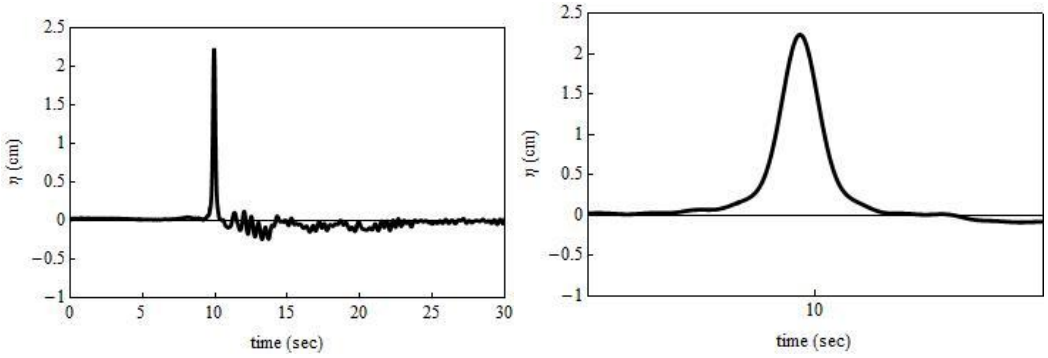

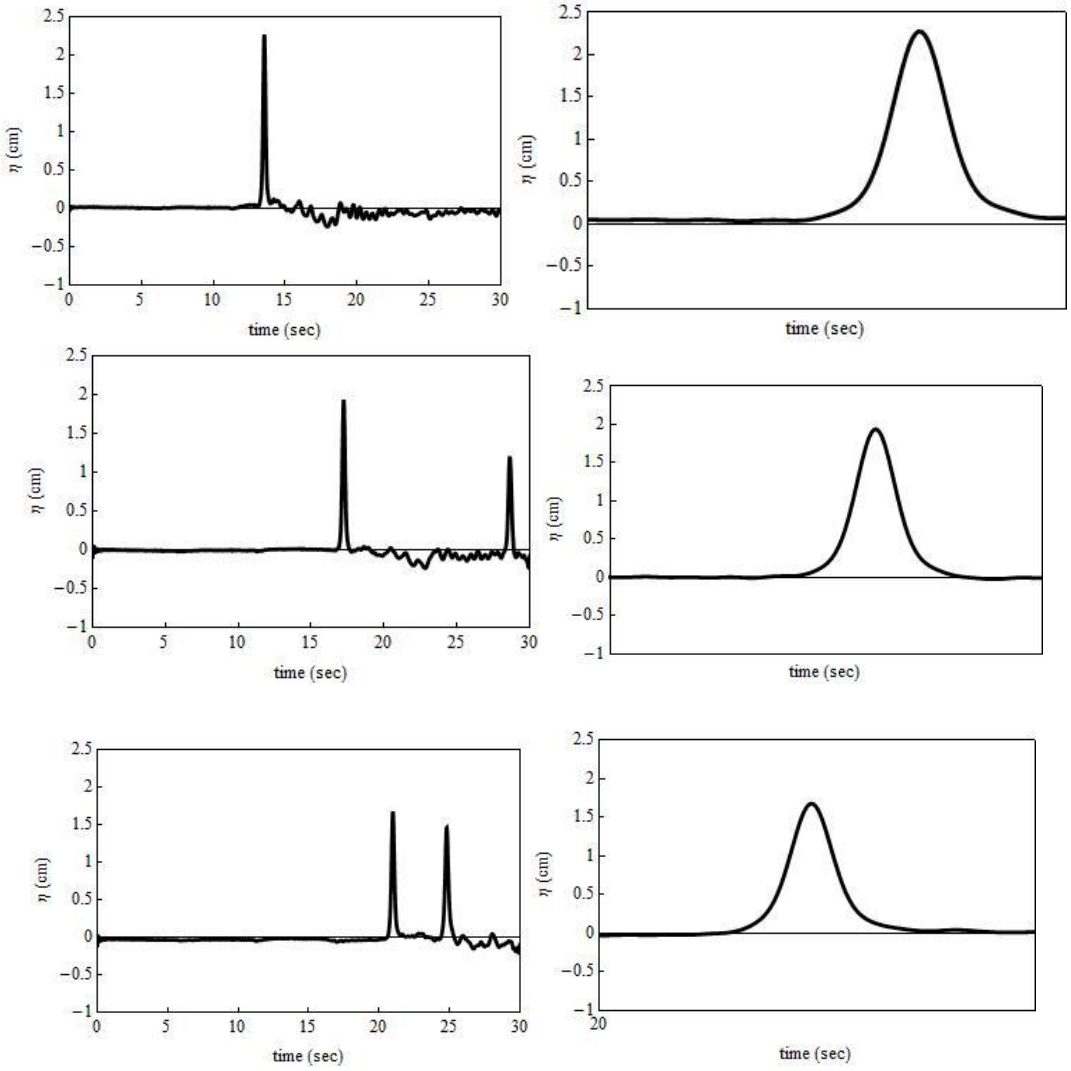

Figure 17 – Data from Experiment 8

Much like in Experiment 7, this experiment seems to indicate a leading peak followed by a period of little to no oscillations. By zooming in on these peaks, we see again that it appears to be similar to a soliton. A comparison of this observed wave to a theoretical soliton is shown in Figure 18.

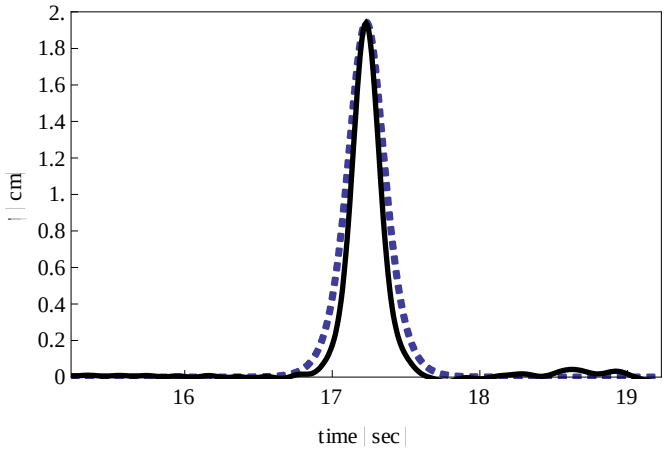

Figure 18 – Comparison of Measured Data to Prediction

Again, this wave is in qualitative agreement to the soliton in (3.8). The gaps caused by the viscous effects are closer in size to those in Experiment 7 as compared to Experiments 1 and 2. This is consistent with the amplitude decay ratio being closer to that of Experiment 7 than to those of Experiments 1 and 2. The measured speed of this experiment, as seen in Table 1, is much larger than any other experiment. Again, this is consistent with theoretical predictions, because the initial amplitude of the wave was the largest of any experiment.

5. Application to Tsunamis

Here we use Sections 2 and 3 as a framework for looking at recent tsunamis. For actual tsunamis in the ocean, we neglect bathymetry and assume a constant ocean depth of 4000 m. This depth gives a wave speed of approximately 200 m/s. In the ocean, the appropriate value of L used to calculate the times for which the asymptotic approximation applies is not well-defined, because actual earthquake motions are complicated. The value of L corresponds to the displacement from the earthquake that causes the tsunami. For example, the 2004 Indian Ocean tsunami was caused by an ocean floor displacement of approximately 15 m. Using this value for L, we find that the long-time approximation applies within one hundredth of a second. Therefore, for any measurable time, the approximations will potentially apply to ocean tsunamis.

In studying the 2004 Indian Ocean tsunami, the National Oceanic and Atmospheric Administration was able to create a computer imaging of how the tsunami waves traveled and evolved throughout the oceans. A full video can be found at http://nctr.pmel.noaa.gov/animations/sumatraGlobe.mpg. Sample images from that simulation are shown in Figure 19 below.

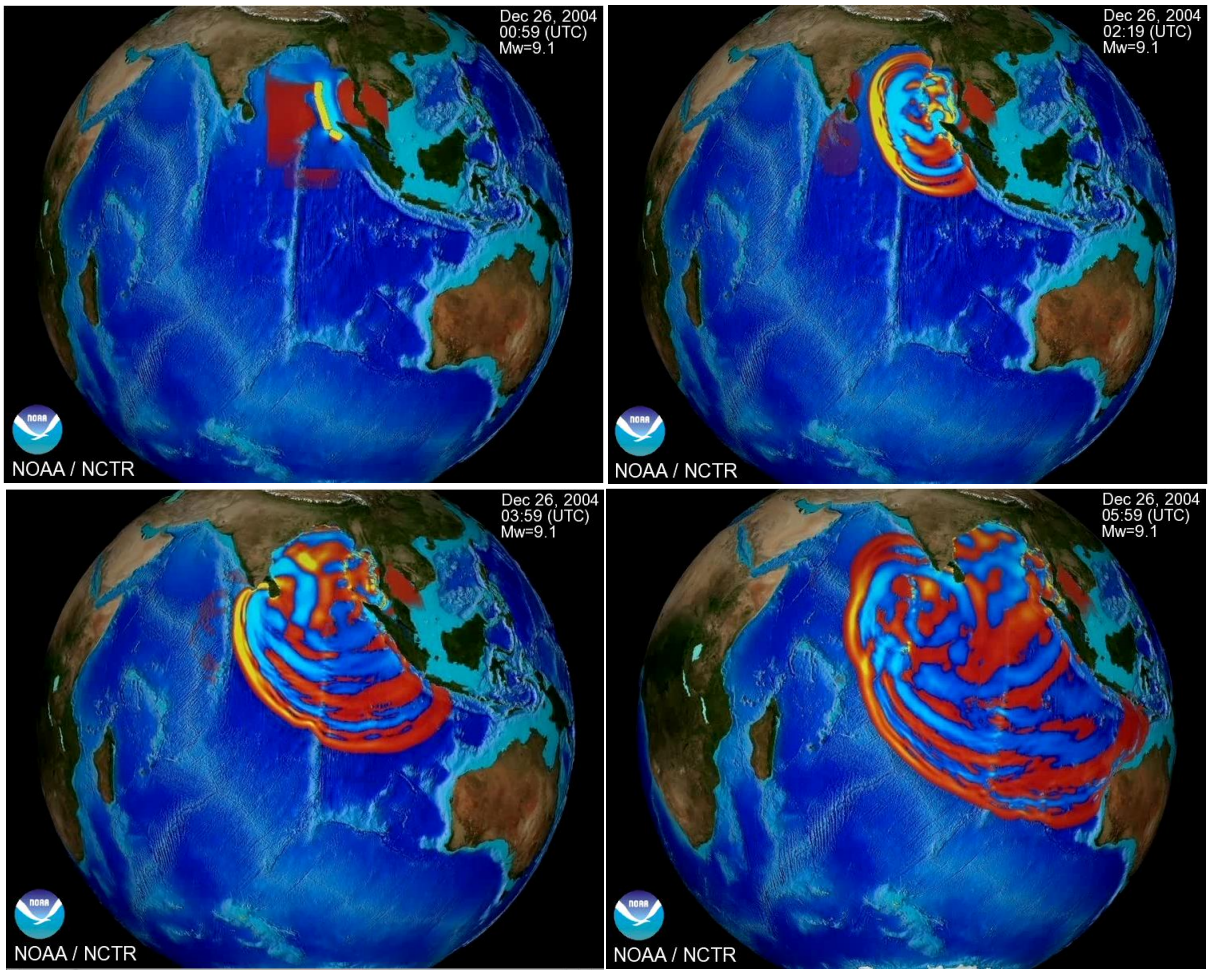

Figure 19 – NOAA Computer Simulation of 2004 Indian Ocean Tsunami (2011)

The four images approximately correspond to times $T = 0, 1.5, 3,$ and 5 hours after the earthquake. In the images, red, orange, and yellow coloring in the waves represents wave amplitudes above sea level, with orange representing smaller amplitudes than yellow, and red representing smaller amplitudes than orange. Bright blue coloring represents wave amplitudes below sea level. From this coloring, we can observe a similar pattern to what theory from Section 3 predicts that we should see – a high wavefront followed by several smaller oscillatory waves behind the front. The high wavefront represents the Airy function that we expect to see very close to the front of the wave, and the oscillatory waves behind the front are the damped cosine waves we expect to see in the trailing region. The westward-propagating wave is similar to the data that we observed in Section 4.5, which involved the nearby water being forced upward by a force. In this case, the water was forced upward by a large earthquake.

In the above discussion, we assumed that the ocean floor was a smooth, constant depth. However, this is not the case, especially in the areas approaching the shore. The continental shelf rises on a slope from the largest ocean depth to a level of zero depth at the shoreline. As the tsunami reaches the continental shelf, the depth of the water decreases. This causes the speed of the tsunami to decrease, because its speed $c \sim \sqrt{gh}$. Figure 20 illustrates this phenomenon.

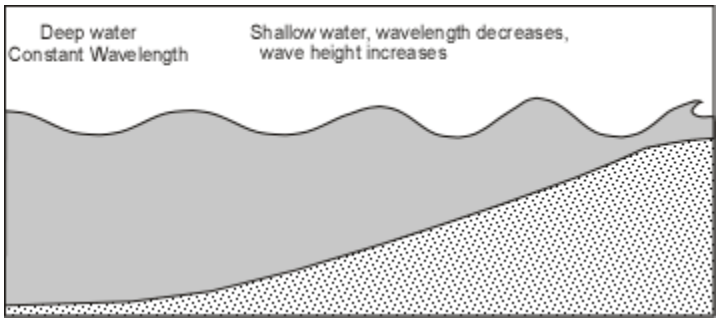

Figure 20 – Representation of Waves at the Continental Shelf (Nelson, 2010)

Furthermore, the waves have the same period and energy as when they hit the continental shelf. Therefore, in order for the wave speed to decrease, the wavelength must decrease as well. This forces more water into the same distance between crests, causing the wave height above the surface to increase. Therefore, waves that may have had extremely small amplitudes in the open ocean can have very large amplitudes when close to shore, causing the common “storm surge” observed when tsunamis reach land.

6. Conclusion

Through our analysis, we have found that in order to know the properties of a shallow-water wave's propagation, we must know the initial condition of the wave. In the laboratory, these conditions can be easily measured, based either on our method of wave generation or on the data that we record. However, in the open ocean, this means we must know the exact conditions of the earthquake that causes the tsunami, which is very hard, if not impossible, to measure at the time of the earthquake. Therefore, it is hard to use this method for tsunami prediction; rather, we can use it to understand tsunamis after they have happened. Regardless of initial data, the speed is about $\sqrt{gh}$, so we can predict fairly accurately when the tsunami will hit a given coastline.

From this analysis, it appears that in the controlled environment of the laboratory, the behavior of waves appears to follow what is predicted by our approximations. In our experiments that we created solitons, the propagating wave had many of the properties that we expected. It held a soliton shape while not undergoing many changes in either speed or amplitude. Also, for experiments with the plate in which we can estimate the original conditions based on the actions performed, the wave again exhibited the same properties that we expected from theory.

For ocean data, we were also able to observe that the behavior of the wave is similar to what we expected from the theory predictions. The solutions to the KdV equation that we discussed show that the wave front is a large peak from an Airy function followed by a period of rapid oscillation trailing the front. When we look at the ocean data from the 2004 Indian Ocean tsunami, we find that in the direction of propagation, the wave front is a large peak and is followed by a region of rapid oscillatory waves.

In this analysis, we neglected viscous effects, and our Fourier Transform solutions neglected nonlinear interactions and bathymetry. Future study could investigate how bathymetry near individual coastlines, which focuses and defocuses wave energy.

References

Ablowitz, M.J., and Segur, H. 1981. *Solitons and the Inverse Scattering Transform*. Philadelphia: S.I.A.M.

Dean, R.G., and Dalrymple, R.A. 1991. *Water Wave Mechanics for Engineers and Scientists*. London: Imperial College Press.

Hammack, J.L. 1973. *A Note on Tsunamis: Their Generation and Propagation in an Ocean of Uniform Depth*. J. Fluid Mech. Vol. 60, pp. 769-799.

Hammack, J.L. and Segur, H. 1974. *The Korteweg-deVries equation and water waves.* J. Fluid Mech. Vol 65, pp. 289-314.

Kreyzig, E. 1999. *Advanced Engineering Mathematics, 8th Edition.* New York: Wiley and Sons.

Nelson, S. 2010. *Natural Disasters: Tsunamis*. http://www.tulane.edu/~sanelson/geol204/tsunami.htm.

NOAA Center for Tsunami Research. 2011. *Tsunami Event – December 26, 2004 Indonesia (Sumatra)*. http://nctr.pmel.noaa.gov/indo_1204.html.

Russell, J. S. 1844. *Report on Waves, Report of the 14th Meeting of the British Association for the Advancement of Science, held in York in September 1844*, 311-391 plus 11 plates.

Stoker, J.J. 1957. *Water Waves: The Mathematical Theory with Applications*. New York: Interscience Publishing.

Stokes, G.G. 1847. *On the theory of oscillatory waves.* Trans. Camb. Phil. Soc. 8, 441.

Strauss, W. 2008. *Partial Differential Equations: An Introduction, 2nd Edition.* New York: Wiley and Sons.

Vasan, V. 2011. Private communication.

Academic Vita

MARK E. WALSH

Local Address: 48 Atherton Hall ▪ University Park, PA 16802
Permanent Address: 143 Opalwood Court ▪ Bethel Park, PA 15102
mew5067@psu.edu ▪ (412) 780-5282

EDUCATION

Bachelor of Science in Physics & Bachelor of Science in Mathematics Expected May 2011
The Pennsylvania State University, University Park, PA
Schreyer Honors College
Thesis Title: The Propagation of Shallow-Water Waves
Thesis Supervisor: Dr. Diane Henderson

WORK EXPERIENCE

UNDERGRADUATE RESEARCHER 2009 – Present
Dr. Diane Henderson, Department of Mathematics, Penn State University
- Ran experiments on the generation and development of one-dimensional wind-blown water waves
- Conducted experiments on the evolution of waves with randomly generated phase shifts
- Conducted experiments on propagation of shallow-water waves

UNDERGRADUATE RESEARCHER 2009
Dr. Robert Enick, Department of Chemical and Petroleum Engineering, University of Pittsburgh
- Reviewed scientific papers detailing methods to predict viscosities of large hydrocarbons
- Developed graphs reflecting prediction methods at various temperatures and pressures

COLLEGIATE & COMMUNITY INVOLVEMENT

SCHREYER HONORS COLLEGE
Schreyer Honors College Student Council 2007-Present
SHO TIME Lead Mentor 2009-2010

PENN STATE MOCK TRIAL ASSOCIATION 2007-Present
President 2010-Present

EAGLE SCOUT 2006
Boy Scout Troop 215, Bethel Park, PA

ACADEMIC ACHIEVEMENTS

Braddock Scholarship – Eberly College of Science
Academic Excellence Scholarship – Schreyer Honors College
Physics Department – Department of Physics
Dean's List